View Article Online
View Journal

Green Chemistry

Cutting-edge research for a greener sustainable future

Accepted Manuscript

This article can be cited before page numbers have been issued, to do this please use: S. Vrabl, K. Bangert, E. F. Semeraro and W. Kroutil, *Green Chem.*, 2026, DOI: 10.1039/D6GC01139J.

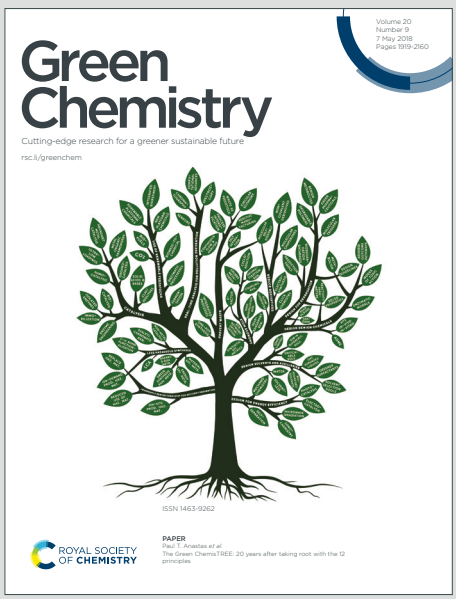

Green Foundation Box

View Article Online
DOI: 10.1039/D6GC01139J

1. Regio- and stereoselective C-H oxidation of free fatty acids is achieved by an enzyme catalyst just at the expense of H_2O_2 in aqueous buffer at room temperature leading to water as the only co-product. Due to the developed variant in this study bearing 43 mutations, substrate concentrations up to 150 mM were used leading to the optically enriched a-hydroxylated fatty acids in high isolated yield.

2. The stability, expressibility and activity of the enzyme catalyst was increased to a practical level reaching TONS of 48000, which is the highest number reported for ahydroxylases.

3. The numbers now have reached values of interest for application. The concept is probably unbeatable as just H_2O_2 is the oxidant and H_2O the co-product and a biodegradable enzyme is used as catalyst in buffer. Next steps may be process engineering which is outside the scope.

View Article Online
DOI: 10.1039/D6GC01139J

ARTICLE

Combining Rational Design and Computational Tools in Multi-Parameter Enzyme Engineering to Increase the Fitness of a CYP152 Peroxygenase for α-Hydroxylation of Fatty Acids

Received 00th January 20xx,
Accepted 00th January 20xx

DOI: 10.1039/x0xx00000x

Stephan Vrabl,[a] Klara Bangert,[a] Enrico F. Semeraro,[b,c,d] and Wolfgang Kroutil*[a,c,d]

Enzymes of the CYP152 family have the potential to upgrade fatty acids to α-hydroxy acids by regio- and stereoselective hydroxylation using hydrogen peroxide as the oxidant and forming water as the sole by-product. To achieve such transformations with relevant productivity, a high tolerance towards hydrogen peroxide is required. By designing a minimal library targeting oxidation-prone residues with high solvent exposure and introducing mutations to improve expression/stability identified by a computational strategy (PROSS), the hydrogen peroxide tolerance of the CYP152 peroxygenase $PO_{SP\alpha}$ was improved up to four-fold. Of the 12 generated enzyme variants, V3-P04 demonstrated the most pronounced improvements across the investigated parameters, exceeding the parent in terms of hydrogen peroxide tolerance, expression yields, and specific activity for the α-hydroxylation of octanoic acid. The superior performance of variant V3-P04 was further underlined in preparative-scale experiments for the functionalisation of heptanoic acid (50 mM), octanoic acid (150 mM), nonanoic acid (100 mM), and 9-decenoic acid (75 mM) where it reached turnover numbers unmatched by the wildtype enzyme of up to 48,333.

[a] Department of Chemistry, University of Graz, Heinrichstraße 28, 8010 Graz, Austria.
E-mail: Wolfgang.Kroutil@uni-graz.at
[b] Department of Molecular Biosciences, University of Graz, Humboldtstraße 50, 8010 Graz, Austria
[c] BioTechMed Graz, 8010 Graz, Austria
[d] Field of Excellence BioHealth, University of Graz, 8010 Graz, Austria
† Footnotes relating to the title and/or authors should appear here.
Supplementary Information available: [details of any supplementary information available should be included here]. See DOI: 10.1039/x0xx00000x

Introduction

C–H Functionalisation enables the introduction of handles at non-activated carbons, directly accessing target molecules whose synthesis would otherwise require multiple steps.[1-3] Although numerous transition metal-catalysed functionalisation approaches have been described, targeted activation of a single C–H bond continues to be challenging for these catalysts.[4] One strategy for selective C–H bond activation is the introduction of molecular recognition elements that force an orientation between substrate and ligand in which a single C–H bond remains accessible for catalysis.[5-7] This is especially optimised in the active sites of enzymes[8] leading to remarkable regio-, chemo-, and stereo-selectivity.[9-17] Among the most extensively studied enzyme classes capable of performing C–H functionalisation reactions are cytochromes P450 (CYPs), which can catalyse the monooxygenation of aliphatic (sp^3) and aryl (sp^2) C–H bonds.[18-23] CYPs have shown to be outstanding catalysts for the selective oxyfunctionalisation of complex organic molecules, making them powerful tools, particularly for late-stage functionalisation.[3, 24-28] However, their dependence on molecular oxygen, cofactors for electron donation [NAD(P)H], and often auxiliary proteins for electron relay complicates their use on preparative scale.[29-31] These limitations may be circumvented by exploiting a shortcut in the catalytic cycle of CYPs, the so-called peroxide shunt pathway, for which hydrogen peroxide (H_2O_2) can act as oxygen- and electron donor enabling the formation of the reactive Fe(IV) oxo species, thereby circumventing the need for additional cofactors or auxiliary proteins, and forming water as the sole by-product.[21, 32-34] While most CYPs require prior engineering to effectively utilise hydrogen peroxide, some have been reported to natively act as peroxygenases, such as unspecific peroxygenases (UPOs)[24, 34-37] or CYP152s.[38, 39] The use of hydrogen peroxide is advantageous in terms of process cost and complexity. However, H_2O_2-mediated enzyme inactivation, caused either by oxidation of sensitive amino acid residues or by degradation of the porphyrin ring (haem-bleaching), can impair catalytic performance.[40] This has been identified as a key issue when working with peroxygenases and different strategies have been employed to reduce peroxide-mediated deactivation. For instance, maintaining low hydrogen peroxide concentrations throughout the reaction, either by continuous feeding or *in situ* generation of the oxidant, has proven successful for mitigating catalyst inactivation.[41-57] Alternatively, enhancing enzyme durability through engineering can lead to improved stability and tolerance toward certain reagents. Targeting residues within the active site pocket of peroxygenases was shown to be a viable strategy for enhancing the hydrogen peroxide stability of both CYPs and UPOs.[58, 59] Similarly, studies focusing on introducing peroxygenase activity by engineering the active site or access tunnel of non-native peroxygenases have reported that the introduced mutations also affected the H_2O_2-stability of the generated variants.[33, 60] In a different approach, all methionine residues of the enzyme

View Article Online
DOI: 10.1039/D6GC01139J

$P450_{BM-3}$ were replaced with their less oxidation-prone analogue norleucine.[61] Although inactivation was not reduced for the resulting variant, the replacement did lead to an enhancement in peroxygenase activity.

In previous studies, the P450 peroxygenase from *Sphingomonas paucimobilis* ($PO_{SPα}$, CYP152B1)[62-64] proved an excellent catalyst for the regioselective α-hydroxylation of fatty acids, achieving high optical purity (*ee* up to >99%).[65] However, stability in the presence of H_2O_2 was suggested to be a limiting factor. By improving stability toward H_2O_2 – e.g., through engineering of oxidation-sensitive residues – without altering the enzyme's high selectivity, the generation of a more durable and efficient catalyst for the selective synthesis of α-hydroxy fatty acids was envisioned, which would allow to reduce the amount of catalyst needed.

Results and discussion

Structure-guided variant design

To generate a variant of $PO_{SPα}$ with improved hydrogen peroxide stability, oxidation-prone residues with high solvent exposure were selected for mutation. For this purpose, the per-residue solvent accessible surface area (SASA) was calculated for all cysteine-, methionine-, and tyrosine residues present in the protein (Figure 1, complete list in Table S1).[66] The three feasible residues with the highest SASA values – namely Y356, Y214, and C260 – were selected for mutation. C361 was excluded as it acts as proximal ligand coordinating to the haem-iron. The targeted amino acids were replaced by less oxidation-sensitive residues, leading to the design of one single variant [$PO_{SPα\ C260H}$ (identifier: V1)] and two triple variants [$PO_{SPα\ Y214V\ C260H\ Y356V}$ (identifier: V2), $PO_{SPα\ Y214Q\ C260H\ Y356Q}$ (identifier: V3)]. Wildtype enzyme and variants were heterologously expressed in *E. coli* with a GST tag and purified by affinity chromatography. To determine whether the introduced mutations improved the enzyme stability toward hydrogen peroxide, the peroxygenases were incubated for two hours with 20 mM H_2O_2 in potassium phosphate buffer [100 mM, pH 7.4, 15% (v/v) glycerol]. Residual peroxide was afterwards removed by addition of catalase, and remaining intact enzyme was determined by measuring cysteine-coordinated Fe-haem centres *via* CO-difference spectroscopy.[67] Indeed, all three variants showed a significantly higher percentage of intact enzyme compared to the parent, for

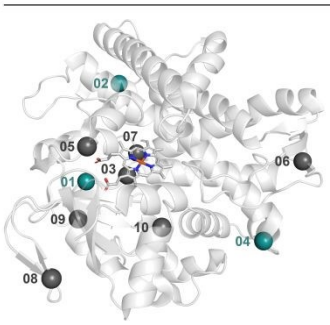

Entry	Amino Acid	Position	SASA [%]
01	Tyr	356	46
02	Tyr	214	36
*03	Cys	361	31
04	Cys	260	25
05	Met	69	23
06	Tyr	384	18
07	Met	102	16
08	Met	304	16
09	Tyr	58	14
10	Tyr	317	13

Figure 1: Solvent accessible surface area (SASA) for cysteine-, methionine-, and tyrosine residues in $PO_{SPα}$ calculated using PyMOL [Protein Data Bank (PDB): 3AWM]. The ten residues with the highest solvent exposure are shown as spheres. Residues selected for mutation are highlighted in teal. *Proximal cysteine residue required for catalysis.

which 52% of unaltered enzyme was detected after the treatment (Table 1). The best result was obtained with the triple variant V3, which preserved 88% of intact reaction centres. This represents an inactivation of only 12% at the conditions used,

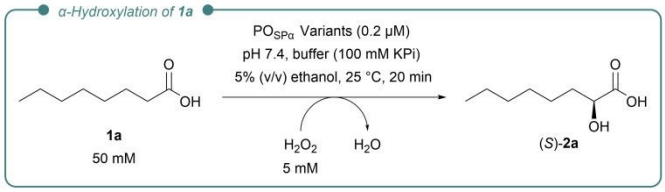

Scheme 1: α-Hydroxylation of octanoic acid (**1a**) to (*S*)-2-hydroxyoctanoic acid [(*S*)-**2a**] by $PO_{SPα}$-variants.

corresponding to a four-fold improvement compared to the parent enzyme, for which 48% inactivation was observed under the same conditions. V1 and V2 behaved comparable to each other, showing an approximately two-fold improved stability under the assay conditions employed. To determine if the introduced mutations affected the catalytic performance of $PO_{SPα}$, the α-hydroxylation of octanoic acid (**1a**) as a model substrate was investigated (Scheme 1, Table 1). Specific activities for the oxidation of **1a** were gratifyingly mostly comparable to the wt for V3 and V1. Furthermore, the two triple variants displayed slightly lower optical purity for the formation of (*S*)-**2a**, reaching 97% *ee* compared to 98-99% of the wt. Although hydrogen peroxide

Table 1: Characterisation of $PO_{SPα}$ wt and variants V1-3 based on hydrogen peroxide stability, expression yields, and specific activity and stereoselectivity for the α-hydroxylation of **1a** to **2a**.

Variant Identifier	Mutations	Remaining intact enzyme [%][a]	Expression Yield [mg][b]	Spec. Activity [U/mg][c]	*ee* **2a** [%][d]
wt	-	52 ± 2	9.1	2.8 ± 0.2	99 ± 0.2 (*S*)
V1	C260H	78 ± 1	9.1	3.0 ± 0.3	98 ± 0.3 (*S*)
V2	Y214V/C260H/Y356V	79 ± 2	5.1	2.3 ± 0.1	97 ± 1.6 (*S*)
V3	Y214Q/C260H/Y356Q	88 ± 2	4.3	2.8 ± 0.3	97 ± 0.3 (*S*)

[a] Remaining, relative intact enzyme concentrations after two-hour incubation in the presence of 20 mM H_2O_2 in potassium phosphate buffer [100 mM, pH 7.4, 15% (v/v) glycerol], 25 °C, 400 rpm. Triplicate determination. [b] Amount of purified protein obtained from cultivation in 660 mL LB-medium. [c] Reaction conditions: 0.2 µM peroxygenase, 50 mM **1a**, and 5 mM H_2O_2 in KPi buffer [100 mM, pH 7.4, 5% (v/v) ethanol], in 2 mL microcentrifuge tubes for 20 minutes at 25 °C and 400 rpm. Triplicate determination. [d] Determined by GC using a chiral phase for a reaction with 10 mM substrate, 3 µM peroxygenase, continuous H_2O_2-addition (1.5 eq, 100 mM stock solution, 12.5 µL/h, over 12 h), in KPi-buffer [1 mL, 100 mM, pH 7.4, 5% (v/v) ethanol] inside 1.5 mL glass GC-vials under shaking (400 rpm, 21 °C, 15 h).

View Article Online
DOI: 10.1039/D6GC01139J

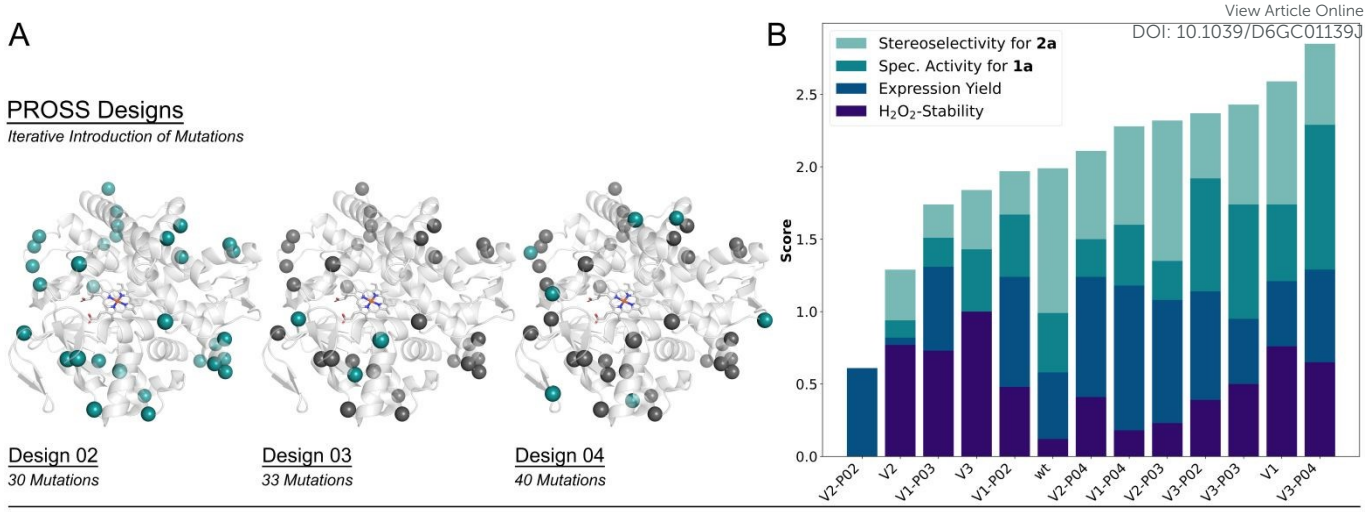

Figure 2: (A) PROSS Designs 02-04 of $PO_{SP\alpha}$ with mutated residues highlighted as spheres. Iterative design process is indicated by different coloured spheres (teal = added mutation, grey = mutation taken over from previous design). (B) Graphical representation of $PO_{SP\alpha}$ variant scoring based on H_2O_2-stability, expression yields, specific activity for the functionalisation of **1a**, and stereoselectivity for the formation of **2a** (Performance score, Table 2).

Table 2: Characterisation of combined $PO_{SP\alpha}$ variants.

Entry	PROSS Design	Variant identifier	Remaining intact enzyme [%][a]	Rel. Expression Yield [%][b]	Spec. Activity [U/mg][c]	*ee* **2a** [%][d]	Performance score[e]
01		V1-P02	67 ± 1	134	2.8 ± 0.1	97 ± 2.3 (*S*)	1.96
02	02	V2-P02	47 ± 1	117	2.1± 0.1	96 ± 2.0 (*S*)	0.61
03		V3-P02	63 ± 3	133	3.4± 0.3	97 ± 0.8 (*S*)	2.38
04		V1-P03	77 ± 1	113	2.4± 0.1	96 ± 1.9 (*S*)	1.74
05	03	V2-P03	57 ± 3	145	2.6± 0.1	99 ± 0.1 (*S*)	2.32
06		V3-P03	68 ± 4	99	3.4 ± 0.1	98 ± 0.2 (*S*)	2.43
07		V1-P04	55 ± 2	161	2.8± 0.1	98 ± 0.3 (*S*)	2.27
08	04	V2-P04	64 ± 1	142	2.5± 0.0	98 ± 0.8 (*S*)	2.11
09		V3-P04	74 ± 1	121	3.7± 0.1	97 ± 1.5 (*S*)	2.85

[a] H_2O_2-Stability: Remaining relative intact enzyme in the presence of 20 mM H_2O_2 in potassium phosphate buffer [100 mM, pH 7.4, 15% (v/v) glycerol], 25 °C, 400 rpm after two-hour incubation. Triplicate determination. [b] Rel. amount of purified protein obtained from cultivation in 660 mL LB-medium compared to the wt. [c] Reaction conditions: 0.2 µM peroxygenase, 50 mM **1a**, 5 mM H_2O_2 in KPi buffer [100 mM, pH 7.4, 5% (v/v) ethanol], in 2 mL microcentrifuge tubes at 25 °C, 400 rpm, 20 minutes. Triplicate determination. [d] Determined by GC using a chiral phase after derivatisation to its methyl ester. [e] Overall score based on partial scores assigned for each of the four investigated parameters.

stability was improved substantially by targeting solvent-exposed, oxidation-sensitive residues for mutation, it was noticed that the soluble expression levels were impaired for the two triple variants V2 and V3. Thus, the gain achieved by improved stability was diminished by the lower expression level, which was addressed in a next step.

Improvement of heterologous expression using PROSS

To address the issue of reduced soluble expression, the sequence of $PO_{SP\alpha}$ was submitted to the Protein Repair One-Stop Shop (PROSS) webserver provided by the Weizmann Institute of Science.[68] PROSS is a computational strategy designed for the automated and unsupervised generation of enzyme variants with improved melting temperatures and, crucially for us, higher soluble bacterial expression. The algorithm first identifies feasible mutations for every position in the target protein by eliminating amino acids that are rare in the natural diversity for a given position. Then, Rosetta computational mutation scanning is used to determine which of the feasible mutations lead to a reduced energy (ΔΔG) compared to the wildtype. Finally, potentially stabilising mutations are combined using Rosetta combinatorial sequence design. To avoid loss of activity/selectivity, amino acid residues within the enzyme's active site and access tunnel were excluded from mutation. Output designs were generated in an iterative fashion, whereby every subsequent design contained all mutations of the previous one (Figure 2, A). Thus, Design 02 had 30 mutations, Design 03 three more, and Design 04 additional seven mutations. The output designs 02 to 04 were selected according to the provided guidelines and combined with mutations introduced in the first round (Table 2; e.g., variant V1 combined with PROSS design P02 is variant V1-P02). Indeed, soluble expression levels could be recovered or even improved beyond wildtype expression. These new combined variants were again evaluated regarding hydrogen peroxide stability and specific catalytic activity (Table 2). Values for specific activity were found to be between 2.1 to 3.7 U/mg and interestingly also highest for V3-derived variants. To deduce the overall best-

performing catalyst from all the collected data, partial scores (s_p) were assigned for each of the four investigated parameters (H_2O_2-stability, expression yield, specific activity for oxidation of **1a**, and stereoselectivity for formation of **2a**). These partial scores were then summed up to give an overall score (performance score, s) for each variant [Figure 2, B; additional details are provided in the Supplementary Information (SI)]. The highest score was reached by variant V3-P04, which outperformed the wildtype enzyme in terms of H_2O_2-stability (74 ± 1%), expression yields (121%), and specific activity (3.7 ± 0.1 U/mg).

Analytical-scale α-hydroxylation of medium-chain fatty acids

Two variants were chosen for the subsequent experiments, namely variant V3, which showed the highest hydrogen peroxide tolerance under the conditions employed, and variant V3-P04, which performed best when considering all parameters investigated. These two were evaluated for the analytical-scale biotransformation of octanoic acid **1a** at varied substrate concentration and compared to the wt (Table 3). Reactions were performed at 50, 75 and 100 mM substrate concentration in a fed-batch setup; thus, hydrogen peroxide was added continuously throughout the reaction using a syringe pump (1.5 equivalents over 12 h). At 50 and 75 mM of substrate, the parent enzyme (wt) as well as both variants reached completion (>99% conv.). At 100 mM **1a**, variant V3-P04 reached the highest conversion, showing improved performance compared to the parent (116% of the wt). Although H_2O_2-stabiltiy was substantially improved for variant V3, V3 reached conversions comparable to the parent enzyme. Running the oxyfunctionalisation for medium-chain fatty acids **1b-d** (Table 4), a similar trend was observed for **1c** and **1d**, whereby V3-P04 outperformed the wildtype at increased substrate loading. For these substrates, variant V3 reached lower conversions compared to the parent. Regarding the functionalisation of **1b**, all three investigated peroxygenases reached comparable conversions irrespective of substrate loading.

Table 3: α-Hydroxylation of **1a** to **2a** with selected $PO_{SPα}$ variants at varied substrate concentration.

Substrate [mM]	Variant	Conv.[a] [%]	**1b** + **2b**[b] [%]	**2a** [%]	*ee*$_{2a}$[c] [%]
50	wt	>99	8	92	98 (*S*)
	V3	>99	3	97	97 (*S*)
	V3-P04	>99	6	94	97 (*S*)
75	wt	>99	3	97	96 (*S*)
	V3	>99	2	98	96 (*S*)
	V3-P04	>99	4	96	96 (*S*)
100	wt	74	1	73	96 (*S*)
	V3	73	1	72	96 (*S*)
	V3-P04	86	2	84	95 (*S*)

Reaction conditions: 3 µM peroxygenase, 50-100 mM **1a**, continuous H_2O_2-addition (1.5 eq, 200-400 mM stock solution, 31 µL/h, over 12 h), in KPi-buffer [1 mL, 100 mM, pH 7.4, 5% (v/v) ethanol] inside 1.5 mL glass GC-vials under shaking (400 rpm, 21 °C, 15 h). Duplicate determination. [a] Conversion and composition determined by GC using calibration after derivatisation with BSTFA-TMCS. [b] Overoxidation products. [c] Determined by GC using a chiral phase after derivatisation to its methyl ester.

Table 4: Conversions [%] for the analytical-scale α-hydroxylation of **1b-d** with selected $PO_{SPα}$ variants.

View Article Online
DOI: 10.1039/D6GC01139J

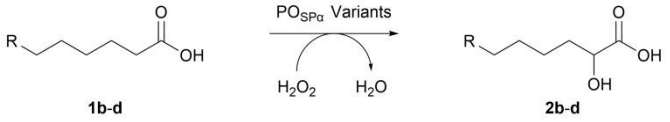

b R = -CH_3 **c** R = -CH_2-CH_2-CH_3 **d** R = -CH_2-CH_2-CH=CH_2

Substrate	Variant	Conv [%][a] Substrate Loading 50 mM	75 mM	100 mM
1b	wt	66	44	27
	V3	64	38	26
	V3-P04	53	45	22
1c	wt	>99	>99	24
	V3	>99	70	5
	V3-P04	>99	>99	58
1d	wt	>99	44	9
	V3	>99	29	1
	V3-P04	>99	66	15

Reaction conditions: 3 µM peroxygenase, 50-100 mM **1b-d**, continuous H_2O_2-addition (1.5 eq, 300-400 mM stock solution, 21-31 µL/h, over 12 h), in KPi-buffer [1 mL, 100 mM, pH 7.4, 5% (v/v) ethanol] inside 1.5 mL glass GC-vials under shaking (400 rpm, 21 °C, 15 h). Duplicate determination. [a] Conversion determined by GC using calibration after derivatisation with BSTFA-TMCS.

To further elucidate the variants' behaviour in high oxidative-stress environments, biotransformations were performed in batch at 25 and 50 mM **1a**, adding one equivalent of H_2O_2 at the onset of the reaction (Table S2). In this case, substrate conversions were significantly impaired, and neither variant managed to exceed the parent enzyme. This shift in performance can be explained by catalyst inactivation caused by haem-degradation, which involves the reaction of haem compounds II and III with additional molecules of hydrogen peroxide, ultimately resulting in the formation of biliverdin under the release of haem-bound iron.[40, 69, 70] Enzyme inactivation due to haem degradation is therefore likely more severe in a batch setup, where effective H_2O_2 levels are higher. This indicates that our approach of targeting oxidation-sensitive residues with high solvent-exposure did not mitigate peroxide-mediated haem-degradation, and continuous oxidant addition (or generation) remains necessary for reaching high productivities. Additionally, when investigating the H_2O_2-mediated enzyme inactivation, we consciously chose a simplified setup in the absence of substrate to avoid the contribution of multiple parameters to the deactivation. This might explain discrepancies between the inactivation data and the variants' performance in the analytical-scale biotransformations, as the carboxylic acid substrate is involved in the activation of hydrogen peroxide in CYP152 peroxygenases.

In the fed-batch reactions with **1a**, we observed a minimal but reproducible decrease in optical purity measured as *ee* of about 2% (e.g., 98% to 96%) with increasing substrate loading (Table 3). Additionally, besides the desired α-hydroxylated product (*S*)-**2a**, low amounts of heptanoic acid **1b** and 2-hydroxyheptanoic

View Article Online
DOI: 10.1039/D6GC01139J

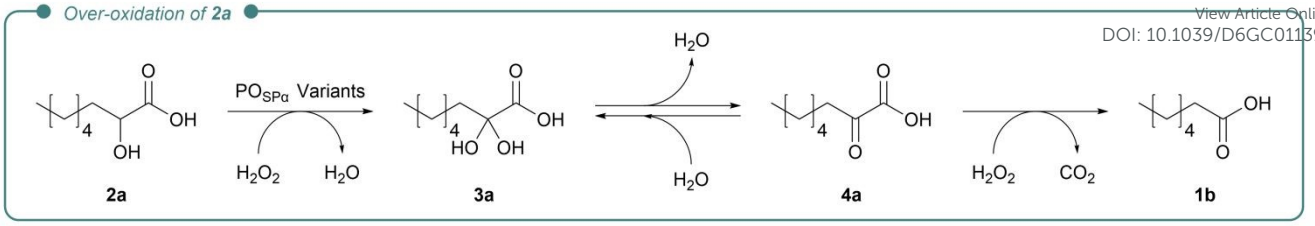

Scheme 2: Over-oxidation of **2a** by $PO_{SPα}$ variants. Peroxygenase-mediated oxidation of **2a** to **3a** followed by formation of **4a** under the release of a molecule of water and finally decarboxylation to **1b** in the presence of H_2O_2.

Table 5: E-Values of selected $PO_{SPα}$ variants for the over-oxidation of **2a**.

Variant	Conv. [%][a]	*ee* **2a** [%][b]	E-Value[c]
wt	63	82 (*S*)	7
V3	63	85 (*S*)	8
V3-P04	67	76 (*S*)	5

Reaction conditions: 3 µM peroxygenase, 10 mM *rac*-**2a**, continuous H_2O_2 addition (1.5 eq, 133 mM stock solution, 12.5 µL/h, over 12 h), in 1 mL KPi buffer [100 mM, pH 7.4, 5% (v/v) ethanol] inside 1.5 mL glass GC-vials under shaking (400 rpm, 21 °C, 15 h). Triplicate determination. [a] Conversion and composition determined by GC using calibration after derivatisation with BSTFA-TMCS. [b] Determined by GC using a chiral phase after derivatisation to its methyl ester. [c] Determined from conversion and *ee* using the ENANTIO online tool (http://biocatalysis.uni-graz.at/biocatalysis-tools/enantio).

acid **2b** were detected in biotransformations of **1a**. The formation of **1b** may be explained by peroxygenase-catalysed over-oxidation of **2a** to the corresponding geminal diol **3a**, followed by dehydration leading to the α-keto acid **4a**, and finally – by decarboxylation in the presence of H_2O_2 – to the shorter-chain fatty acid **1b** (Scheme 2).[71-73] Due to the difference in *ee* observed at higher substrate loading, we suspected that the $PO_{SPα}$-mediated over-oxidation of **2a** may display an enantiopreference for the conversion of the minor formed (*R*)-enantiomer, leading to an improvement of the optical purity of (*S*)-**2a**, the main enantiomer formed in the hydroxylation, at extended time. To determine whether the peroxygenase-mediated over-oxidation of the α-hydroxy acid **2a** is responsible for this change in *ee*, *rac*-**2a** was investigated as substrate (Table 5). Indeed, the three enzymes tested showed a preference for the oxidation of (*R*)-**2a** with E-values of 5-8, explaining the varied values of optical purity observed for the functionalisation of **1a** (Table 3). Thus, the optical purity of the α-hydroxylation product (*S*)-**2a** is improved by the subsequent stereocomplementary oxidation of (*R*)-**2a** in a cooperative cascade achieving an increase of *ee* of **2a** over time. To explain the low enantioselectivity of $PO_{SPα}$ for the over-oxidation of **2a**, molecular docking of both enantiomers of **2a** in the active site of $PO_{SPα}$ was performed using rigid receptor docking in Glide (Figure 3). For both (*S*)-**2a** and (*R*)-**2a** two distinct poses were observed. In all cases, the ligands coordinated with R241 through hydrogen bonding and salt bridges. R241 is located above the enzyme's reaction centre and is conserved within members of the CYP152 family, where it is involved in both substrate binding/positioning and the activation of hydrogen peroxide. Here, hydrogen bonding with R241 occurred either exclusively with the ligands' carboxylate groups (Figure 3, A and C) or with both the carboxylate- and α-hydroxy groups of **2a** (Figure 3, B and D). Furthermore, in all four poses, hydrogen bonding between the α-hydroxy group of **2a** and the oxygen of the simulated reactive Fe(IV) oxo species (compound I) was observed. Since over-oxidation of **2a** requires homolytic cleavage of the $C_α$–H bond (followed by OH rebound formally leading to oxygen incorporation and the formation of **3a**), the $C_α$-proton of **2a** needs to be in proximity to the reactive Fe(IV) oxo species for catalysis to occur. Regarding (*S*)-**2a**, only one of the two observed poses can be envisioned to lead to a productive orientation where C–H bond cleavage can occur (Figure 3, A). Whereas, in the case of (*R*)-**2a**, both observed ligand orientations could lead to over-oxidation due to the proximity of the $C_α$ proton to the oxygen of compound I (2.9 and 3.2 Å, respectively; Figure 3, C and D). This difference in binding between the two enantiomers of **2a** in the active site of $PO_{SPα}$ may indicate the moderate enantioselectivity of the enzyme for oxidation of (*R*)-**2a**.

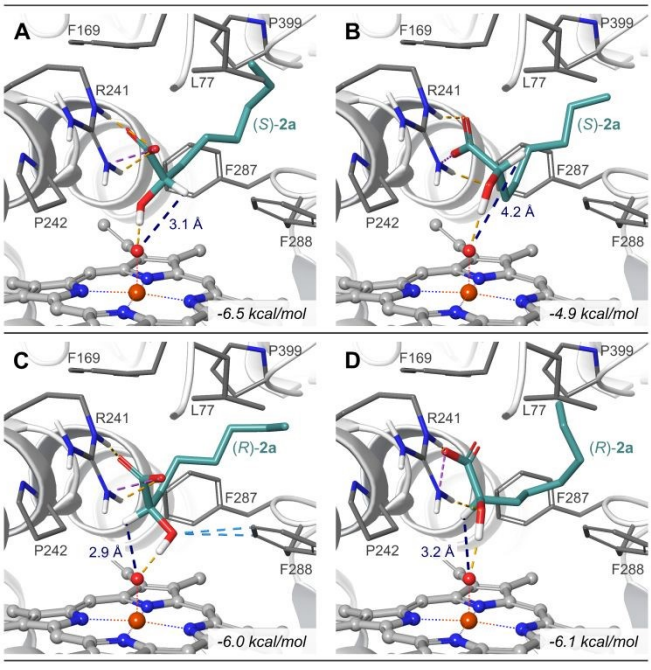

Figure 3: Molecular docking of (*S*)-**2a** (A and B) and (*R*)-**2a** (C and D) in the active site of $PO_{SPα}$ (PDB: 3AWM) using rigid receptor docking with Glide. Ligands are highlighted in teal. Hydrogen bonding is indicated by yellow dotted lines, salt bridges are indicated by purple dotted lines, and aromatic hydrogen bonding is indicated by light blue dotted lines. Distances between the $C_α$-proton of **2a** and the oxygen of compound I are shown in blue. Docking scores are given in kcal/mol for each entry.

View Article Online
DOI: 10.1039/D6GC01139J

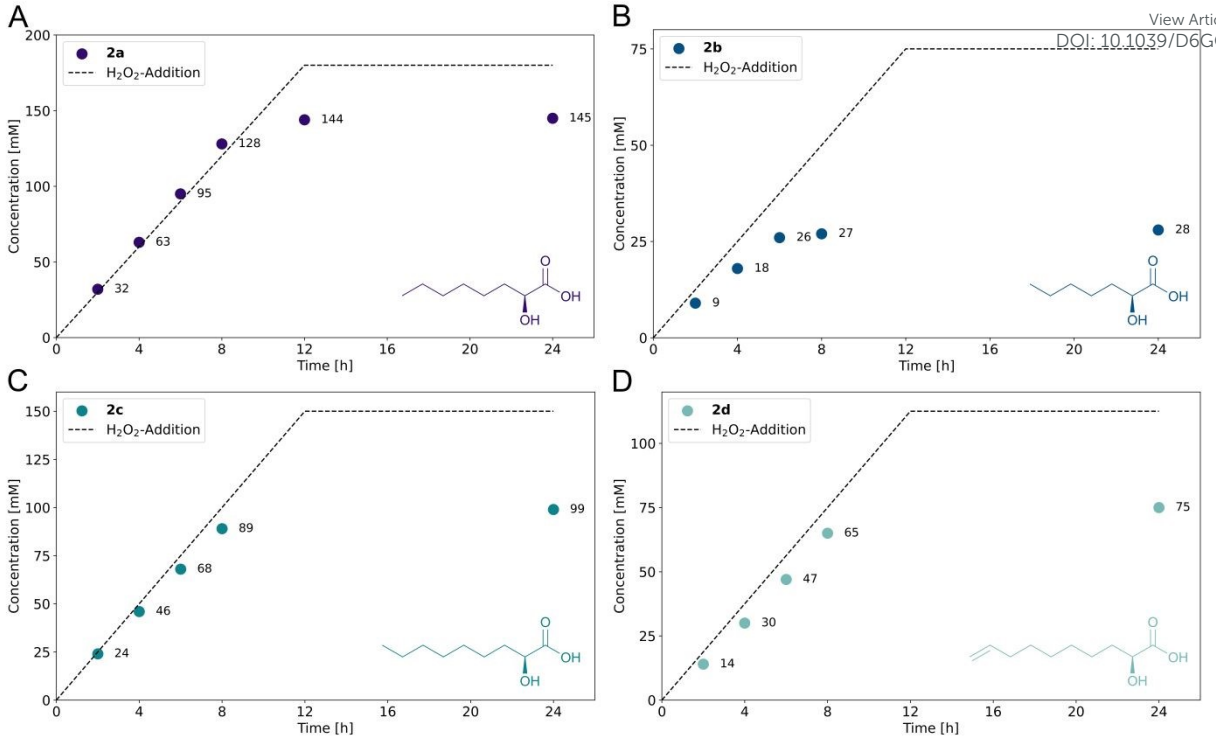

Figure 4: Reaction progression for the preparative-scale oxyfunctionalisation of medium-chain fatty acids using V3-P04. (A) Formation of **2a** over time (150 mM loading of **1a**). (B) Formation of **2b** over time (50 mM loading of **1b**). (C) Formation of **2c** over time (100 mM loading of **1c**). (D) Formation of **2d** over time (75 mM loading of **1d**).

Preparative-scale oxyfunctionalisation of medium-chain fatty acids

Preparative-scale biotransformations were performed for fatty acids **1a**-**d** (Table 6). Reactions were conducted at 20 mL scale and substrate concentrations were selected based on results obtained in analytical-scale experiments (Table 4), except for **1a**, for which it was noticed that elevated concentrations of up to 150 mM were suitable. Hydrogen peroxide was fed continuously to the reaction, and reaction progress was monitored over time for a better understanding of the performance of the catalyst (Figure 4). For substrates **1a**, **1c**, and **1d**, the rate of product formation matched the rate of addition of hydrogen peroxide during the first eight hours of feeding. At this time, most of the substrate was consumed, and reaction rates started to decrease. This indicates that feeding rates were well-matched to the catalyst, leading to immediate consumption of the H_2O_2 added. It further suggests that under the conditions used, uncoupling phenomena are not an issue for V3-P04.[74, 75] The oxyfunctionalisation of **1a**, performed at a substrate loading of 150 mM, reached almost completion (97% conversion) after 24 hours, which corresponds to a turnover number (TON) of 48,333 for the $PO_{SP\alpha}$ variant V3-P04. This significantly exceeds previously reported values for the wildtype enzyme, highlighting the improved performance of V3-P04 at high substrate loading. Furthermore, the reaction course shows that incubation times could be further reduced with V3-P04, since the reaction was completed after 12 hours. Transformations for **1c** and **1d** reached completion after 24 hours and the α-hydroxylated products were obtained with high isolated yields (87-91%) and in high optical purity [*ee* 94-95% (*S*)]. Interestingly, the functionalisation of **1b** required a lower H_2O_2 addition rate (using a lower concentration of H_2O_2) compared to the other substrates, but still the catalyst was unable to match the half H_2O_2 addition rate of **1c** (Figure 4B). This lead most likely to an accumulation of non-transformed H_2O_2 which subsequently resulted in enzyme inactivation and a drop in reaction rate after six hours, with a final conversion of 56% after 24 hours. All isolated products were obtained in high optical purity [*ee* 89-95% (*S*)]. The absolute configuration for alcohol (*S*)-**2a** was deduced by comparison of elution order on a chiral phase with previous reports.[65] The absolute configuration of (*S*)-**2b**, was determined by comparison of the specific optical rotation of the isolated product with literature.[76] For the C9:0 hydroxylated product (*S*)-**2c**, we determined the specific optical rotation {$[\alpha]_D^{25}$ = +4.32° (c = 3.15, $CHCl_3$)} as well, but noticed that the sign was opposite to literature reports {$[\alpha]_D^{24}$ = -3.48°

Table 6: Preparative-scale biotransformations of medium-chain fatty acids with V3-P04.

Substrate	Substr. conc. [mM]	Conv.[a] [%]	TON	*ee* [%][b]	Isol. Yield [mg]
1a	150	97	48,333	94 (*S*)	385 (80%)
1b	50	56	9,333	89 (*S*)	36 (25%)
1c	100	>99	33,333	95 (*S*)	302 (87%)
1d	75	>99	25,000	94 (*S*)	253 (91%)

Reaction conditions: 3 µM peroxygenase, 50-150 mM **1a**-**d**, continuous H_2O_2-addition (1.2-1.5 eq, 250-600 mM stock, 500 µL/h, over 12 h), in 20 mL KPi-buffer [100 mM, pH 7.4, 5% (v/v) ethanol] inside a 100 mL round-bottom flask using stirring (400 rpm, 21 °C, 24 h). [a] Conversion and composition determined by GC using calibration after derivatisation with BSTFA-TMCS. [b] Determined by GC using a chiral phase after derivatisation to its methyl ester.

View Article Online
DOI: 10.1039/D5GC01370J

(c = 3.16, $CHCl_3$)}.[77] However, the literature report refers to another paper[78] for the optical rotation, which does actually not include the target molecule **2c** at all. We argue that the optical rotation values for the (*S*)-enantiomers of α-hydroxylated fatty acids (C6, C7, C8, C10) measured in chloroform are exclusively reported with positive signs.[76, 79-82] Furthermore, all optically enriched (*S*)-products obtained in this study show the same elution order on GC using a chiral phase.[76, 79-82] Finally, an inversion of the stereoselectivity of $PO_{SPα}$ just for C9:0 is unlikely; it should be the same as for C8:0 and C10:1. From the three indications (optical rotation, elution order, enzyme stereospecificity), we therefore conclude that the major enantiomer of **2c** isolated in the preparative experiment is also (*S*)-configured. The absolute configuration of (*S*)-**2d**, bearing a terminal C=C double bond, was determined by chemical reduction of the isolated product to its saturated analogue and comparison of elution order on a chiral phase with literature reports.[65]

Comparison with other synthetic approaches

α-Hydroxy fatty acids are relevant compounds for the pharmaceutical, cosmetic, and polymer industry, making their selective generation from low-cost, readily available fatty acids highly desirable.[24, 83, 84] While chemical methods often suffer from insufficient selectivity, some chemical approaches for the α-hydroxylation of fatty acids, or more generally carboxylic acids, have been reported. For instance, by activation of the carboxylate group of a fatty acid substrate, employing a strong base such as lithium diisopropylamide (LDA), and subsequent addition of oxygen, the corresponding α-hydroxy acid can be formed.[85] Alternatively, hydroxylation of an α-chlorination intermediate has been successful for the selective synthesis of α-hydroxy fatty acids.[86] Initial α-chlorination can be achieved by employing, for instance, trichloroisocyanuric acid (TCCA). Other chemical strategies for the α-oxidation of carboxylic acids utilise the formation of an enediolate intermediate that is subsequently oxidised using a free radical such as TEMPO (2,2,6,6-tetramethylpiperidine 1-oxyl).[87, 88] While these chemical strategies for the synthesis of α-hydroxy acids can offer sufficient regioselectivity, they yield the desired products exclusively in racemic form. Biocatalytic approaches are attractive alternatives to more traditional chemical processes for the selective hydroxylation of carboxylic acids, and in particular fatty acids. Regarding the direct C–H oxyfunctionalisation of saturated fatty acids, CYPs have been widely employed as this is often their natural activity. In this case, hydroxylation in terminal positions (ω-1 to ω-3) has been predominantly reported, even though their high stability makes terminal C–H bonds particularly challenging.[24, 84, 89] In-chain hydroxylation is rarer, but has been described, for instance, in the oxyfunctionalisation of decanoic acid to 5-hydroxydecanoic acid using a class VII CYP.[89] The formation of such in-chain hydroxylation products is of particular interest as they can be further converted to their corresponding lactone derivatives. Both terminal and in-chain hydroxylation of saturated fatty acids have also been described for UPOs.[51, 90, 91] Regarding the biocatalytic α-hydroxylation of saturated fatty acids, members of the CYP152 family show the highest potential. They act as peroxygenases, thus requiring H_2O_2 as the only reagent, thereby avoiding the need for additional cofactors or electron transfer partners. Of all CYP152 members described, $PO_{SPα}$ shows the highest regio- and stereoselectivity for the formation of α-hydroxy acids. In comparison to our previous study,[65] we have now improved the stability of the enzyme to be able to reach a 15% higher TON (48,333), which means that about 15% less catalyst is needed to reach similar product formation as reported before, which subsequently means that fewer reagents are required for its production. The here reported variant of $PO_{SPα}$, V3-P04 clearly outperforms the parent enzyme for the oxyfunctionalisation of **1a** and enables the efficient functionalisation of other medium-chain fatty acids at high substrate loadings (≥75 mM). For a closer comparison of the current biocatalytic approach to chemical processes, green chemistry metrics were determined, and key reaction parameters were highlighted (Table 7). The E-Factor (Environmental Factor), which provides information on the amount of waste produced in a process, and the Atom Economy, describing the relative mass of reactants of a given reaction that are incorporated into the final product, were considered suitable green metrics for this purpose. For each literature reference the reaction yielding the highest amount of α-hydroxylated carboxylic acid product was selected (see Scheme S3 in the Supplementary Information). Furthermore, it should be noted that for entries 3 and 4 the final products are the TEMPO-substituted acids, not the free α-hydroxy acids. Ideally, when calculating the E-Factor, the whole process up to the isolation of the final product should be considered.

Table 7: Comparison of synthetic approaches for the preparation of α-hydroxy acids from carboxylic acids.

Entry	Substrate	Reactants	Steps[a]	Temp. [°C][b]	Yield [%]	E-Factor[c]	Atom Economy[d]	Ref.
1	C8:0	V3-P04, H_2O_2	1 (1)	21	80	71.1	89.9	This work
2	C18:0	LDA, O_2	2 (1)	-78	47	210.4	56.6	85
3[e]	C7:0	$LiNEt_2$, LiCl, Fe cat.[f], TEMPO	2 (1)	-78	51	74.5	50.9	87
4[e]	2-(*p*-tolyl)acetic acid	Fe cat.[f], TEMPO	1 (1)	60	97	17.3	99.7	88
5	C18:0	TCCA, KOH/H_2O	2 (2)	80	68	30.0	79.1	86

[a]Total amount of reaction steps. Number of individual steps where intermediate isolation is required is given in parentheses. [b]Required reaction temperature (the temperature deviating most from ambient is given in the case multiple temperatures applied in the process). [c]Calculated based on Equation S4 (see SI). [d]Calculated based on Equation S5 (see SI). [e]Data provided for these entries refers to the formation of the TEMPO-substituted products and not the free α-hydroxy acids. [f]Iron catalyst. For entry 3: Ferrocenium hexafluorophosphate ([Fc]PF_6), for entry 4: Iron acetate [$Fe(OAc)_2$] + phenanthroline ligand.

However, as in some cases insufficient details were provided in literature for work up- and purification steps, only components employed in the actual reactions were considered for calculations (further details are provided in the Supplementary Information). The here presented α-hydroxylation of fatty acids achieved the best Atom Economy for the reactions that lead to the α-hydroxylated product (Entry 1). Formerly, a higher atom economy is only reached in the process leading to the TEMPO-adduct (entry 4).[88] Furthermore, although the E-Factor of 71.1 in our reaction is higher than in entries 4 and 5,[86,88] the bulk of the formed waste is in our case just water (95%). The here presented process achieved the second highest yields, requires only a single reaction step, and employs ambient reaction temperatures, making it less energy demanding. And finally, and probably rather important, the enzymatic reaction is the only one leading to the desired product in enantiomerically enriched form.

Conclusions

Combining rational structure-guided design targeting oxidation-sensitive surface-exposed amino acids with a computational tool to improve expressibility, a variant of $PO_{SP\alpha}$ was generated that significantly outperformed the wildtype enzyme for the regio- and stereoselective α-hydroxylation of naturally occurring, medium-chain fatty acids. In the evaluation of the variants, multiple parameters had to be considered, such as the stability against H_2O_2, the specific activity, the expressibility, and the optical purity of the product. Additionally, the catalyst showed a complementary stereoselectivity for the oxidation of the α-hydroxy acid, thus the product of the first step, which led overall to a cooperative follow-up reaction, leading to an improvement of the *ee* of the α-hydroxy acid.
The catalyst developed paves the way to efficient synthesis of optically enriched α-hydroxy acids in buffer just at the expense of H_2O_2 as oxidant.

Author contributions

S. V. and K. B. contributed to experimental investigation. S. V., K. B., and W. K. contributed to the conceptualization of the project. S. V. and K. B. contributed to data curation. S. V. and E. S. contributed to the formal analysis of data. S. V. and W. K. contributed to writing the original draft. W. K. contributed by providing resources and supervising the project.

Conflicts of interest

The authors declare no conflict of interest.

Data availability

The data supporting this article have been included as part of the Supplementary Information. Supplementary information: Tables S1-S3, Figures S1-S39 including NMR spectra and further experimental details. See DOI: [URL format https://doi.org/DOI]
References cited in the Supplementary Information are listed in the article's reference list.[67, 92, 93]

Acknowledgements

The University of Graz and the Field of Excellence BioHealth are acknowledged for financial support. S.V. and W.K. acknowledges the Austrian Science Fund (FWF) 10.55776/COE17 within the Cluster of Excellence Circular Bioengineering. K.B. and W.K. received funding from the European Union's Horizon 2020 research and innovation programme under Marie Skolodowska-Curie grant agreement ID: 956621.

Notes and references

1. T. Rogge, N. Kaplaneris, N. Chatani, J. Kim, S. Chang, B. Punji, L. L. Schafer, D. G. Musaev, J. Wencel-Delord, C. A. Roberts, R. Sarpong, Z. E. Wilson, M. A. Brimble, M. J. Johansson and L. Ackermann, *Nat. Rev. Methods Primers*, 2021, **1**, 43.
2. C.-M. Che, V. K.-Y. Lo, C.-Y. Zhou and J.-S. Huang, *Chem. Soc. Rev.*, 2011, **40**, 1950-1975.
3. E. Romero, B. S. Jones, B. N. Hogg, A. Rué Casamajo, M. A. Hayes, S. L. Flitsch, N. J. Turner and C. Schnepel, *Angew. Chem., Int. Ed.*, 2021, **60**, 16824-16855.
4. B. Liu, A. M. Romine, C. Z. Rubel, K. M. Engle and B.-F. Shi, *Chem. Rev.*, 2021, **121**, 14957-15074.
5. S. Das, C. D. Incarvito, R. H. Crabtree and G. W. Brudvig, *Science*, 2006, **312**, 1941-1943.
6. C. Sambiagio, D. Schönbauer, R. Blieck, T. Dao-Huy, G. Pototschnig, P. Schaaf, T. Wiesinger, M. F. Zia, J. Wencel-Delord, T. Besset, B. U. W. Maes and M. Schnürch, *Chem. Soc. Rev.*, 2018, **47**, 6603-6743.
7. G. Meng, N. Y. S. Lam, E. L. Lucas, T. G. Saint-Denis, P. Verma, N. Chekshin and J. Q. Yu, *J. Am. Chem. Soc.*, 2020, **142**, 10571-10591.
8. C. K. Winkler, J. H. Schrittwieser and W. Kroutil, *ACS Cent. Sci.*, 2021, **7**, 55-71.
9. G. Qu, F. Zhong, J. Xu, X. Huang and Z. Sun, *Green Synthesis and Catalysis*, 2025, DOI: 10.1016/j.gresc.2025.12.002.
10. H. Kries, F. Trottmann and C. Hertweck, *Angew. Chem., Int. Ed.*, 2024, **63**, e202309284.
11. R. Buller, S. Lutz, R. J. Kazlauskas, R. Snajdrova, J. C. Moore and U. T. Bornscheuer, *Science*, 2023, **382**.
12. E. Radley, J. Davidson, J. Foster, R. Obexer, E. L. Bell and A. P. Green, *Angew. Chem., Int. Ed.*, 2023, **62**, e202309305.
13. E. Grandi, F. Feyza Özgen, S. Schmidt and G. J. Poelarends, *Angew. Chem., Int. Ed.*, 2023, **62**, e202309012.
14. P. Lozano and E. García-Verdugo, *Green Chem.*, 2023, **25**, 7041-7057.
15. E. L. Bell, W. Finnigan, S. P. France, A. P. Green, M. A. Hayes, L. J. Hepworth, S. L. Lovelock, H. Niikura, S. Osuna, E. Romero, K. S. Ryan, N. J. Turner and S. L. Flitsch, *Nat. Rev. Methods Primers*, 2021, **1**, 46.

16. U. Hanefeld, F. Hollmann and C. E. Paul, *Chem. Soc. Rev.*, 2022, **51**, 594-627.
17. J. C. Lewis, P. S. Coelho and F. H. Arnold, *Chem. Soc. Rev.*, 2011, **40**, 2003-2021.
18. H. Renata, *Chem. Soc. Rev.*, 2025, **54**, 7913-7932.
19. Y. Wang, H. Pan, F. Wang and C. Shen, *Biotechnol. Bioeng.*, 2023, **121**, 7-25.
20. D. Permana, T. Kitaoka and H. Ichinose, *Biotechnol. Bioeng.*, 2023, **120**, 1725-1745.
21. X. Xu, T. Hilberath and F. Hollmann, *Curr. Opin. Green Sustain. Chem.*, 2023, **39**, 100745.
22. H. Park, G. Park, W. Jeon, J. O. Ahn, Y. H. Yang and K. Y. Choi, *Biotechnol. Adv.*, 2020, **40**, 107504.
23. R. Fasan, *ACS Catal.*, 2012, **2**, 647-666.
24. L. Hammerer, C. K. Winkler and W. Kroutil, *Catal. Lett.*, 2018, **148**, 787-812.
25. V. B. Urlacher and M. Girhard, *Trends Biotechnol.*, 2019, **37**, 882-897.
26. N. D. Fessner, *ChemCatChem*, 2019, **11**, 2226-2242.
27. M. C. White and J. Zhao, *J. Am. Chem. Soc.*, 2018, **140**, 13988-14009.
28. R. V. Espinoza, K. C. Haatveit, S. W. Grossman, J. Y. Tan, C. A. McGlade, Y. Khatri, S. A. Newmister, J. J. Schmidt, M. Garcia-Borràs, J. Montgomery, K. N. Houk and D. H. Sherman, *ACS Catal.*, 2021, **11**, 8304-8316.
29. M. T. Lundemo, S. Notonier, G. Striedner, B. Hauer and J. M. Woodley, *Appl. Microbiol. Biotechnol.*, 2016, **100**, 1197-1208.
30. M. T. Lundemo and J. M. Woodley, *Appl. Microbiol. Biotechnol.*, 2015, **99**, 2465-2483.
31. J. B. van Beilen, W. A. Duetz, A. Schmid and B. Witholt, *Trends Biotechnol.*, 2003, **21**, 170-177.
32. M. N. Podgorski, J. Akter, L. R. Churchman, J. B. Bruning, J. J. De Voss and S. G. Bell, *ACS Catal.*, 2024, **14**, 7426-7443.
33. A. C. Ebrecht, M. S. Smit and D. J. Opperman, *Catal. Sci. Technol.*, 2023, **13**, 6264-6273.
34. G. Grogan, *JACS Au*, 2021, **1**, 1312-1329.
35. D. T. Monterrey, A. Menés-Rubio, M. Keser, D. Gonzalez-Perez and M. Alcalde, *Curr. Opin. Green Sustain. Chem.*, 2023, **41**, 100786.
36. M. Hofrichter and R. Ullrich, *Curr. Opin. Chem. Biol.*, 2014, **19**, 116-125.
37. R. Ullrich, J. Nuske, K. Scheibner, J. Spantzel and M. Hofrichter, *Appl. Environ. Microbiol.*, 2004, **70**, 4575-4581.
38. A. W. Munro, K. J. McLean, J. L. Grant and T. M. Makris, *Biochem. Soc. Trans.*, 2018, **46**, 183-196.
39. Y. Jiang, P. Gong, Z. Li, Z. Li, Y. Li, B. Wang, H. Huang, W. Peng, X. Gao and S. Li, *Angew. Chem., Int. Ed.*, 2025, **64**, e202506614.
40. B. O. Burek, S. Bormann, F. Hollmann, J. Z. Bloh and D. Holtmann, *Green Chem.*, 2019, **21**, 3232-3249.
41. M. Kluge, R. Ullrich, K. Scheibner and M. Hofrichter, *Green Chem.*, 2012, **14**, 440-446.
42. C. E. Paul, E. Churakova, E. Maurits, M. Girhard, V. B. Urlacher and F. Hollmann, *Bioorg. Med. Chem.*, 2014, **22**, 5692-5696.
43. Y. Ni, E. Fernández-Fueyo, A. G. Baraibar, R. Ullrich, M. Hofrichter, H. Yanase, M. Alcalde, W. J. H. van Berkel and F. Hollmann, *Angew. Chem., Int. Ed.*, 2016, **55**, 798-801.
44. S. J. Freakley, S. Kochius, J. van Marwijk, C. Fenner, R. J. Lewis, K. Baldenius, S. S. Marais, D. J. Opperman, S. T. L. Harrison, M. Alcalde, M. S. Smit and G. J. Hutchings, *Nat. Commun.*, 2019, **10**, 4178.
45. S. Bormann, D. Hertweck, S. Schneider, J. Z. Bloh, R. Ulber, A. C. Spiess and D. Holtmann, *Biotechnol. Bioeng.*, 2021, **118**, 7-16.
46. A. Yayci, Á. G. Baraibar, M. Krewing, E. F. Fueyo, F. Hollmann, M. Alcalde, R. Kourist and J. E. Bandow, *ChemSusChem*, 2020, **13**, 2072-2079.
47. H. Kawana, T. Miwa, Y. Honda and T. Furuya, *ACS Omega*, 2022, **7**, 20259-20266.
48. E. Romero, M. J. Johansson, J. Cartwright, G. Grogan and M. A. Hayes, *Angew. Chem., Int. Ed.*, 2022, **61**, e202207831.
49. J. Brehm, R. J. Lewis, T. Richards, T. Qin, D. J. Morgan, T. E. Davies, L. Chen, X. Liu and G. J. Hutchings, *ACS Catal.*, 2022, **12**, 11776-11789.
50. T. Hilberath, R. van Oosten, J. Victoria, H. Brasselet, M. Alcalde, J. M. Woodley and F. Hollmann, *Org. Process Res. Dev.*, 2023, **27**, 1384-1389.
51. P. Gomez de Santos, A. González-Benjumea, A. Fernandez-Garcia, C. Aranda, Y. Wu, A. But, P. Molina-Espeja, D. M. Maté, D. Gonzalez-Perez, W. Zhang, J. Kiebist, K. Scheibner, M. Hofrichter, K. Świderek, V. Moliner, J. Sanz-Aparicio, F. Hollmann, A. Gutiérrez and M. Alcalde, *Angew. Chem., Int. Ed.*, 2023, **62**, e202217372.
52. B. Pogrányi, T. Mielke, A. Díaz-Rodríguez, J. Cartwright, W. P. Unsworth and G. Grogan, *Angew. Chem., Int. Ed.*, 2023, **62**, e202214759.
53. R. J. Lewis and G. J. Hutchings, *Acc. Chem. Res.*, 2024, **57**, 106-119.
54. C.-X. Liu, Z.-W. Zhou, C.-X. Cai, Y.-J. Wei, Z.-P. Yu, X.-Y. Wang and N. Wang, *ACS Applied Materials & Interfaces*, 2025, **17**, 6347-6356.
55. G. V. Sayoga, V. S. Bueschler, H. Beisch, B. Fiedler, D. Ohde and A. Liese, *Electrochem. Commun.*, 2025, **177**, 107949.
56. B. Çiçek, S. N. H. Hadewig, D. Tischler and A. C. R. Ngo, *ChemCatChem*, 2025, **17**, e01099.
57. S. Last, T. Heinks, N. Dietz, S. Koopmeiners, G. Fischer von Mollard, M. J. Weissenborn and J. von Langermann, *Adv. Synth. Catal.*, 2025, **367**, e202500105.
58. Q.-S. Li, J. Ogawa and S. Shimizu, *Biochem. Bioph. Res. Co.*, 2001, **280**, 1258-1261.
59. T. Li, R. Jin, B. Wu, D. Lan, Y. Ma and Y. Wang, *Chin. Chem. Lett.*, 2024, **35**, 108701.
60. M. N. Podgorski and S. G. Bell, *ACS Catal.*, 2025, **15**, 5191-5210.
61. P. C. Cirino, Y. Tang, K. Takahashi, D. A. Tirrell and F. H. Arnold, *Biotechnol. Bioeng.*, 2003, **83**, 729-734.
62. I. Matsunaga, E. Kusunose, I. Yano and K. Ichihara, *Biochem. Biophys. Res. Co.*, 1994, **201**, 1554-1560.
63. S. Gandomkar, A. Dennig, A. Dordic, L. Hammerer, M. Pickl, T. Haas, M. Hall and K. Faber, *Angew. Chem., Int. Ed.*, 2018, **57**, 427-430.
64. D. Giuriato, D. Correddu, G. Catucci, G. Di Nardo, C. Bolchi, M. Pallavicini and G. Gilardi, *Protein Sci.*, 2022, **31**, e4501.
65. K. Bangert, A. Swoboda, S. Vrabl, H. Rudalija, M. Lazzarotto, S. Payer, A. Glieder, C. A. M. R. van Slagmaat, S. M. A. De Wildeman and W. Kroutil, *Green Chem.*, 2024, **26**, 3183-3189.
66. T. Fujishiro, O. Shoji, S. Nagano, H. Sugimoto, Y. Shiro and Y. Watanabe, *J. Biol. Chem.*, 2011, **286**, 29941-29950.

View Article Online
DOI: 10.1039/D6GC01139J

67. F. P. Guengerich, M. V. Martin, C. D. Sohl and Q. Cheng, *Nat. Protoc.*, 2009, **4**, 1245-1251.
68. A. Goldenzweig, M. Goldsmith, Shannon E. Hill, O. Gertman, P. Laurino, Y. Ashani, O. Dym, T. Unger, S. Albeck, J. Prilusky, Raquel L. Lieberman, A. Aharoni, I. Silman, Joel L. Sussman, Dan S. Tawfik and Sarel J. Fleishman, *Molecular Cell*, 2016, **63**, 337-346.
69. B. Valderrama, M. Ayala and R. Vazquez-Duhalt, *Chem. Biol.*, 2002, **9**, 555-565.
70. A. Karich, K. Scheibner, R. Ullrich and M. Hofrichter, *J. Mol. Catal. B: Enzym.*, 2016, **134**, 238-246.
71. A. Olmedo, J. C. d. Río, J. Kiebist, R. Ullrich, M. Hofrichter, K. Scheibner, A. T. Martínez and A. Gutiérrez, *Chemistry – A European Journal*, 2017, **23**, 16985-16989.
72. H. Onoda, O. Shoji, K. Suzuki, H. Sugimoto, Y. Shiro and Y. Watanabe, *Catal. Sci. Technol.*, 2018, **8**, 434-442.
73. A. Dennig, F. Blaschke, S. Gandomkar, E. Tassano and B. Nidetzky, *Adv. Synth. Catal.*, 2019, **361**, 1348-1358.
74. I. G. Denisov, T. M. Makris, S. G. Sligar and I. Schlichting, *Chem. Rev.*, 2005, **105**, 2253-2278.
75. T. L. Poulos, *Chem. Rev.*, 2014, **114**, 3919-3962.
76. K. Weinges, G. Braun and B. Oster, *Liebigs Ann. Chem.*, 1983, **1983**, 2197-2214.
77. S. Sankaranarayanan, A. Sharma and S. Chattopadhyay, *Tetrahedron Asymmetry*, 1996, **7**, 2639-2643.
78. B. Haase and M. P. Schneider, *Tetrahedron Asymmetry*, 1993, **4**, 1017-1026.
79. D. H. S. Horn and Y. Y. Pretorius, *J. Chem. Soc.*, 1954, DOI: 10.1039/JR9540001460, 1460-1464.
80. F. M. Hauser, M. L. Coleman, R. C. Huffman and F. I. Carroll, *J. Org. Chem.*, 1974, **39**, 3426-3427.
81. M. Masuda and K.-i.-c. Nishimura, *Chem. Lett.*, 2006, **10**, 1333-1336.
82. A. Bodlenner, S. M. Glueck, B. M. Nestl, C. C. Gruber, N. Baudendistel, B. Hauer, W. Kroutil and K. Faber, *Tetrahedron*, 2009, **65**, 7752-7755.
83. Y. C. Heng, G. W. J. Wong and S. Kittelmann, *Biotechnology for Biofuels and Bioproducts*, 2024, **17**, 131.
84. F. Tieves and F. Hollmann, *Eur. J. Lipid Sci. Technol.*, 2025, **127**, e70000.
85. F. N. Muralidharan and V. B. Muralidharan, *Chem. Phys. Lipids*, 1984, **34**, 257-263.
86. V. Bertolini, M. Pallavicini, G. Tibhe, G. Roda, S. Arnoldi, L. Monguzzi, M. Zoccola, G. Di Nardo, G. Gilardi and C. Bolchi, *ACS Omega*, 2021, **6**, 31901-31906.
87. E. Dinca, P. Hartmann, J. Smrček, I. Dix, P. G. Jones and U. Jahn, *Eur. J. Org. Chem.*, 2012, **2012**, 4461-4482.
88. T. Tanaka, R. Yazaki and T. Ohshima, *J. Am. Chem. Soc.*, 2020, **142**, 4517-4524.
89. J. Manning, M. Tavanti, J. L. Porter, N. Kress, S. P. De Visser, N. J. Turner and S. L. Flitsch, *Angew. Chem., Int. Ed.*, 2019, **58**, 5668-5671.
90. A. Gutiérrez, E. D. Babot, R. Ullrich, M. Hofrichter, A. T. Martínez and J. C. del Río, *Arch. Biochem. Biophys.*, 2011, **514**, 33-43.
91. A. C. Ebrecht, T. M. Mofokeng, F. Hollmann, M. S. Smit and D. J. Opperman, *Org. Lett.*, 2023, **25**, 4990-4995.
92. R. A. Friesner, J. L. Banks, R. B. Murphy, T. A. Halgren, J. J. Klicic, D. T. Mainz, M. P. Repasky, E. H. Knoll, M. Shelley, J. K. Perry, D. E. Shaw, P. Francis and P. S. Shenkin, *J. Med. Chem.*, 2004, **47**, 1739-1749.
93. M. M. Aboelnga, *RSC Adv.*, 2022, **12**, 15543-15554.

View Article Online
DOI: 10.1039/D6GC01139J

The data supporting this article have been included as part of the Supplementary Information. Supplementary information: Tables S1-S3, Figures S1-S39 including NMR spectra and further experimental details. See DOI: [URL – format https://doi.org/DOI]

References cited in the Supplementary Information are listed in the article's reference list.[67, 92, 93]